Multi-User Spatial Consistency Analysis of Outdoor Massive-MIMO Measurements

Karstensen, Anders; Nielsen, Jesper Ødum; Eggers, Patrick Claus Friedrich; De Carvalho, Elisabeth; Pedersen, Gert Frølund; Alm, Martin; Steinbock, Gerhard

Published in:
I E E E Transactions on Antennas and Propagation

DOI (link to publication from Publisher):
10.1109/TAP.2021.3111411

Publication date:
2022

Document Version
Accepted author manuscript, peer reviewed version

This article has been accepted for publication in IEEE Transactions on Antennas and Propagation. This is the author's version which has not been fully edited and content may change prior to final publication. Citation information: DOI 10.1109/TAP.2021.3111411

Multi-User Spatial Consistency Analysis of Outdoor Massive-MIMO Measurements

Anders Karstensen, Jesper Ø. Nielsen, Patrick C. F. Eggers, Elisabeth De Carvalho, Gert F. Pedersen, Martin Alm, Gerhard Steinböck

***Abstract*—This paper presents a massive multiple-input multiple-output outdoor measurement campaign with bi-directional angular discrimination. Two dynamic user arrays of eight elements each, are measured simultaneously. Multi-user consistency and spatial consistency is important for proper modelling and simulation of dynamic users in massive-MIMO channels. This paper will investigate the common scatterers between two moving users by considering the power contribution from physical objects to each user. Inter-user distance and user alignment in the direction of dominant scatterers are also considered. Paths are estimated from wideband dual directional beam-scanning. A method is developed to group the paths based on delay and angular development along the measured tracks. The estimated delay and angle of each path, along with ray tracing simulations, are used to map the interactions of each path to surrounding walls or objects. The power contributions from objects are compared to determine common scatterers between users, which can cause larger correlation and a reduced MIMO capacity.**

***Index Terms*—Massive-MIMO, Dual user, multi-user consistency, measurement.**

I. Introduction

Massive multiple-input multiple-output (MMIMO) is considered to be a key technology to meet the growing traffic demands for the fifth-generation (5G) cellular systems with its potential for a large increase in throughput and energy efficiency [1]–[3]. Unlike conventional MIMO systems (up to 8 antenna ports in Long Term Evolution-Advanced (LTE-A), MMIMO systems are expected to have base station antenna arrays with tens or hundreds of antenna elements to serve multiple users in the same time-frequency resource [4]. The large potential has sparked wide interest and multiple measurement campaigns to investigate the MMIMO channel. Channel sounding is often used to measure the multiple channels in a MMIMO system. Utilizing a vector network analyzer (VNA) and a virtual array is simple and cost-effective but slow, and cannot capture dynamic channels [5]–[8]. More complex, dedicated channel sounders with mutliple parallel receive and transmit chains can utilize real arrays to measure a large number of links within the coherence time of the channel, and is capable of recording dynamic channels [9]–[11]. Previous works utilized channel sounder with real and virtual arrays to estimate multipath components, both by beamforming and super-resolution techniques like Unitary ESPRIT and SAGE [12]–[16]. The estimated paths and clusters are mapped to structures in the environment to investigate their impact on propagation behaviour. Previous measurement campaigns have observed the predicted capacity gains of MMIMO, but also propagation characteristics like non-stationarity and have investigated spatial consistency and inter-user correlation [8], [11], [17], [18].

In multi-user scenarios, shared clusters between the individual users can reduce the channel vectors' orthogonality and lead to unfavorable channel conditions and reduced capacity [19]–[22]. Clusters can be defined in more than one way [23], [24]. In this paper, a cluster refers to a set of multipath components with similar delay and angles of both arrival and departure. With the introduction of large base station arrays serving multiple users simultaneously, these propagation characteristics need to be considered for realistic modeling and simulation of the MMIMO channel. Ray tracing (RT) and map-based models like the METIS model [25] could support these, but are considered too costly in complexity and simulation time. The widely used channel models like Winner II/Winner+ [26], [27], 3GPP SCM-3D [28], COST2100 [29] and Quadriga [30] were not designed for all the propagation aspects of 5G MMIMO. The work presented in [31], [32] and [33] proposes extensions of current models and addresses spatial consistency with the adoption of cluster visibility regions (VRs) at both the mobile side as well as on the base station side. VR define a confined area in which the cluster is visible and contribute to a user or base-station antenna. An extension to the Quadriga model proposes a inter-user distance-based criteria to determine the level of cluster correlation [33]. The visibility regions of COST2100 proposed in [31], [32] offer a similar distance-based correlation mechanism. However, a recent study comparing the user distance and channel correlation in non line of sight (NLOS) indicates that not only the user distance but also angular separation of dominant paths is important for the correlation in this scenario [34].

Common clusters and their evolution as the users move are generally not considered in current channel models. This needs to be further investigated and understood for realistic modeling and simulation of dynamic multi-user scenarios.

In this work, a large outdoor MMIMO measurement campaign is introduced. The large basestation array and two moving user arrays allow estimation of individual paths by their joint angle of arrival (AoA) and angle of departure (AoD) as observed from the Rx and Tx arrays at the two ends of the

Anders Karstensen, Jesper Ø. Nielsen, Patrick C. F. Eggers, Elisabeth De Carvalho and Gert F. Pedersen are with the Department of Electronic Systems, Aalborg University, Denmark.

Martin Alm and Gerhard Steinböck are with Huawei Technologies Sweden AB.

This article has been accepted for publication in IEEE Transactions on Antennas and Propagation. This is the author's version which has not been fully edited and content may change prior to final publication. Citation information: DOI 10.1109/TAP.2021.3111411

double-directional propagation channel [35]. Wideband dual-directional beam-scanning is applied to estimate path gain, delay and angles from the measurements. A method was developed for grouping these paths across time/movement, and RT is then used to assist in mapping the paths interactions to the surrounding walls and objects. Finally, the scattering walls and objects are analysed in terms of their power contribution to the two users and compared with user channel orthogonality. The observations are summarized and some suggestions for modeling to support multi-user spatial consistency are presented. The main contributions are summarized in the following:

- Analysis of a large measurement and ray tracing campaign in an outdoor environment with an elevated base station array and two simultaneously moving user arrays and bidirectional angular discrimination.
- Single and multi-bounce paths are mapped to the physical environment based on beam-scanning and ray tracing simulations to investigate the link between common clusters and user channel correlation.
- Suggestions for improved multi-user spatial consistency modeling are presented based on observations from analyzed data.

Section II will introduce the measurement system and location. The Beam-scanning method is detailed in Section III. Section IV describes how the paths were estimated from beam-scanning and later mapped to physical objects assisted by ray tracing. Section V details the results from applying path mapping to compare clusters between users. Section VI discusses the results, and Section VII concludes this paper.

II. Measurements

This section describes the array configurations, measurement equipment and the tracks recorded by the mobile user arrays.

A. Array Configuration

The massive Receiver (Rx) array is configured as two stacked Uniform Linear Arrays (ULAs) each consisting of 64 Vivaldi elements [36]. The two rows are separated by 54.5 cm. The elements are grouped in 8 modules of 16 elements each for the sake of the switching structure, which is detailed in Section II-B. The element spacing is 5 cm, or 0.58 wavelength at $3.5\,\mathrm{GHz}$, across both of the $3.2\,\mathrm{m}$ long ULAs. The measured half power beam-width of a Vivaldi element in the array modules are $99.5°$ and $34.5°$ in azimuth and elevation respectively. The Rx array is located on a balcony on the fourth floor of a tall university building, as depicted in Fig. 1.

The two transmitter (Tx) arrays are configured as Uniform Circular Arrays (UCAs) consisting of 8 patch elements each. The array is designed with a radius of $5.1\,\mathrm{cm}$ and element separation of 0.46 wavelengths to allow beam-scanning. Both arrays are mounted on a trolley with large rubber wheels to allow for easy movement and minimal shaking when moving on the asphalt/sidewalk. The arrays are both at the same height of $167\,\mathrm{cm}$ above the ground, and are both aligned and fixed with the walking direction of the trolley to resolve

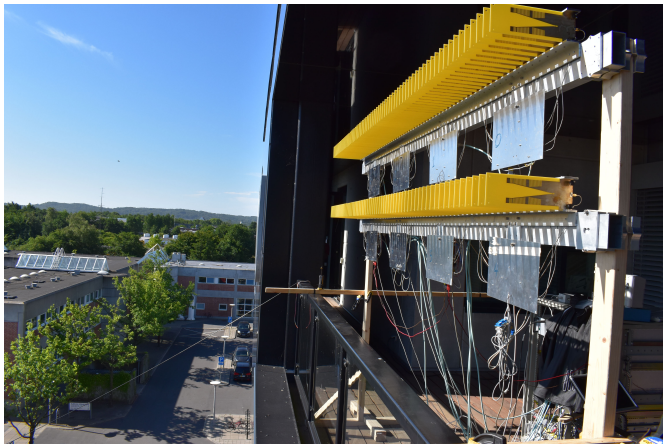

Fig. 1: 2x64 Rx array located on the fourth-floor balcony.

directions after beam-scanning. The Tx-array denoted as Tx1 is connected directly to the Tx-rack (seen in the background of Fig. 2) via short RF-cables. The Tx-array denoted as Tx2 has RF amplifiers on the trolley and is connected to the Tx-rack by optical fibers. With a stationary Tx-rack, Tx1 has about $9\,\mathrm{m}$ of cable for movement, while Tx2 has up to $300\,\mathrm{m}$. One of the identical arrays is depicted in Fig. 2.

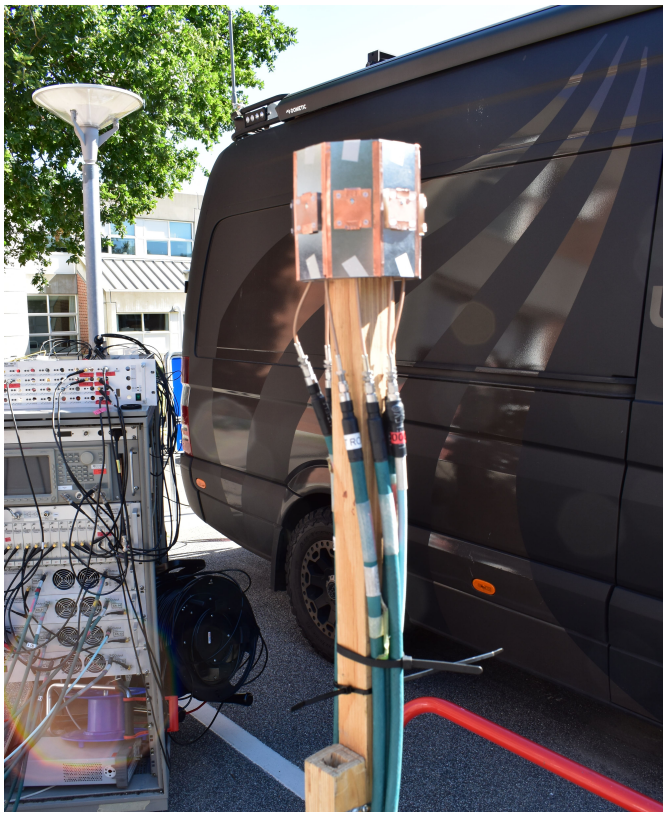

Fig. 2: 8 element circular Tx array

B. Measurement Equipment

The measurement system is based on the correlation based channel sounder developed at Aalborg University (AAU) [37].

This article has been accepted for publication in IEEE Transactions on Antennas and Propagation. This is the author's version which has not been fully edited and content may change prior to final publication. Citation information: DOI 10.1109/TAP.2021.3111411

The carrier frequency is 3.5 GHz and a bandwidth of 100 MHz was measured. The sounder has 16 fully parallel transmitters (user) and 8 fully parallel receivers (base station). The 8 receive channels are each connected to a 1:16 switch so that a total of 128 receive elements can be measured semi-simultaneously. With the 1:16 switching, a snapshot of channel impulse responses of the full 128x16 MIMO channel is recorded in 1.31 ms.

The measurements are recorded in blocks of 15 seconds where 900 snapshots are recorded at a rate of 60 Hz, enough to support Nyquist sampling rate for a slow walking speed of both users, and phased processing of all arrays. During a typical 15-second measurement, the Tx arrays moves by 9 meters, which is one snapshot every 1 cm, or 8.5 snapshots for every wavelength of movement.

The elements of the Tx and Rx arrays are vertically polarized, as the main focus is on spatial cluster behaviour and shared clusters under mobility. The high gain Vivaldi antennas were selected to ensure a sufficient outdoor coverage but does not allow a straight forward way of configuring a dual polarized array, which might be desirable. A dual-polarized setup would further require four times the number of channels, resulting in a large increase in snapshot duration and a lower allowed mobility speed.

The Tx rack is synced to the Rx rack by a fiber optical cable, allowing coherent phase measurements and a Tx-Rx rack separation of about 300 m. As mentioned in Sec. II. A, Tx2 is separated via fiber optical cables (300 m length) from the Tx-rack. Thus the maximum possible distance between Rx and Tx2 is approximately 600 m. For MMIMO, the downlink channel is typically most utilized for high-speed connections, but in this campaign, the uplink channel is measured due to practicality and the structure of the measurement system. Since the propagation channel is reciprocal, the measurement direction does not matter.

C. Measurement Scenarios

An outdoor measurement campaign is designed around the AAU campus at Frederik Bajers Vej in Aalborg, Denmark. The area consists of multiple buildings of mostly two storeys height, with roads and paths in-between the buildings. A map of the area is depicted in Fig. 3, where the location of the base station array and the tracks (blue and red) covered by the two user arrays are drawn on top. At one end of this campus area is a taller building with an open balcony on the fourth floor where the massive base station (Rx) array was placed. The two user (Tx) arrays were moving simultaneously on the ground in between the buildings.

Several long tracks are constructed for Tx2 by concatenating multiple 15-second measurement blocks, as illustrated by the division of the blue tracks in Fig. 3. The short tracks of Tx1 are repeated the number of times it takes Tx2 to complete the long track. Most tracks are in NLOS, but a few tracks or parts of tracks are in line of sight (LOS). Tx1 and Tx2 are always measured simultaneously, and the tracks are designed to have a large variety of inter-user separation and visibility scenarios.

The analysis in this paper will investigate segments of about 1.5 meter movement each from selected measurement blocks

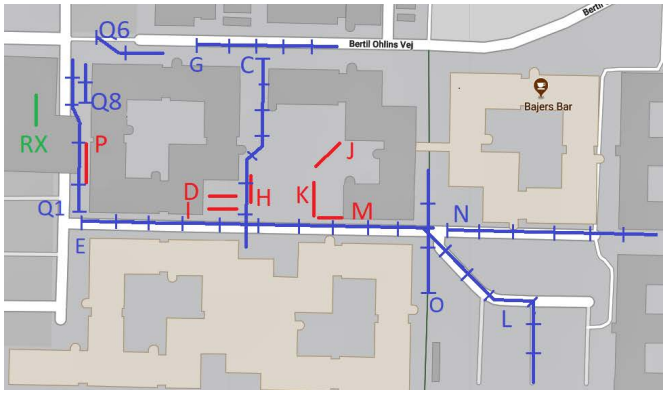

Fig. 3: TX and RX location of all measurement tracks. Red is Tx1, blue is Tx2 and green is the Rx array. Image by Google Maps.

of interest. One Segment is illustrated in Fig. 4, each 1.5 m segment is further split into six equally spaced samples of 9 snapshots each (approximately one wavelength of Tx movement) for beam-scanning. The 9 snapshots are averaged in equation (3) to reduce the effect of small scale fading. Between each analysed sample is about two wavelengths of movement. The paper only presents and discusses a limited set of segments to limit the number of pages. As both Tx arrays are measured simultaneously, the term ”position” will refer to the pair of measured segments or physical location of both Tx arrays. The array locations in the 7 sets of analysed positions are depicted in Fig. 5. Positions 1-4 are from the parallel tracks E and I, these four positions have decreasing and then increasing inter-user distance as Tx2 moves from the street-canyon, past Tx1, and into the open square. Positions 5-7 are from the perpendicular tracks C and D. The main attributes of the chosen positions are detailed below:

- Positions 1 & 5 have medium/large distance and NLOS between the user arrays.
- Positions 2-4 share the same dominant wall reflection, but have different angular alignment to the wall.
- Positions 6 & 7 have different dominant walls, but the walls are closely spaced in angle seen from the base station

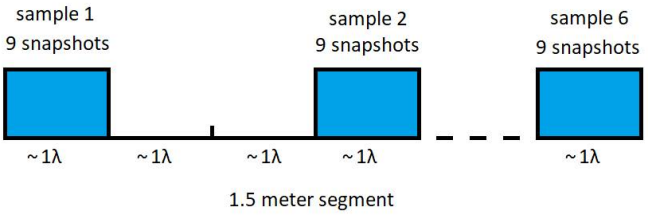

Fig. 4: Breakdown of a segment of 6 samples, each sample (blue) covers 9 snapshots or approximately 1 wavelength of movement. Approximately 2 wavelengths of movement between each sample.

This article has been accepted for publication in IEEE Transactions on Antennas and Propagation. This is the author's version which has not been fully edited and content may change prior to final publication. Citation information: DOI 10.1109/TAP.2021.3111411

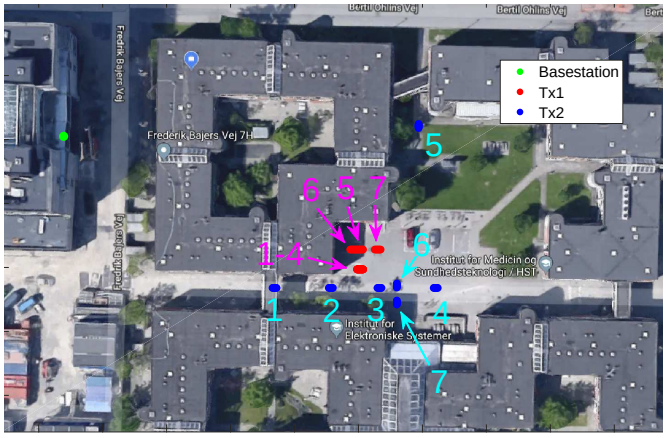

Fig. 5: Rx and Tx array locations in STPs 1-7. Image by Google Maps.

III. Beam-scanning

In this analysis, beam-scanning was performed from the Rx array, as well as from each of the two Tx arrays. The beam-scanning uses only 1 module (16 elements) of the Rx array to reduce angular estimation errors due to possible non-stationarity across the large array. With larger arrays, the angle is susceptible to change depending on cluster visibility at different regions of the array. The result is a dual directional channel characterization for each of the Tx arrays.

The dual directional azimuth power spectrum (APS) is calculated according to the Bartlett beamformer [38], for each single delay index τ:

$$\mathrm{APS}(\theta_{rx}, \theta_{tx}, \tau) = a^* \hat{R}(\tau) a \tag{1}$$

where $\theta_{tx} \in [-180, 179]$ is the AoD in degrees and $\theta_{rx} \in [-90, 90]$ is the AoA in degrees with 0° pointing alog the x-axis in Fig. 5. $()^*$ denotes the complex conjugate transpose and:

$$a = a_{tx}(\theta_{tx}) \otimes a_{rx}(\theta_{rx}) \tag{2}$$

where $\otimes$ denotes the Kronecker product, $a_{tx}(\theta_{tx})$ and $a_{rx}(\theta_{rx})$ is the normalized steering vector of Tx and Rx arrays respectively. The steering vectors are obtained from 3D measurements of the arrays in a multi probe measurement system from MVG [39]. A Hamming window of size M_{rx} is applied to the vector a_{rx} to suppress sidelobes in the APS. In (1), $\hat{R}(\tau)$ is the estimated covariance matrix given by:

$$\hat{R}(\tau) = \frac{1}{T} \sum_{t=1}^{T} y(t, \tau) y^*(t, \tau) \tag{3}$$

where $y(t, \tau)$ is a stacked vector of the $N \times M$ impulse responses at snapshot index t and delay index τ, where each index increment corresponds to $\Delta_t = 16.7\,\mathrm{ms}$ and $\Delta_\tau = 2.5\,\mathrm{ns}$. N is the number of Tx elements, M is the number of Rx elements and $T = 9$ is the number of snapshots included in the estimation.

The single sided power angular spectrum seen from the Tx or the Rx array is obtained by marginalization of the respective other angle domain as follows:

$$\mathrm{P_{rx}}(\theta_{rx}, \tau) = \frac{1}{N_{\theta_{tx}}} \sum_{\theta_{tx}} \mathrm{APS}(\theta_{rx}, \theta_{tx}, \tau) \tag{4}$$

$$\mathrm{P_{tx}}(\theta_{tx}, \tau) = \frac{1}{N_{\theta_{rx}}} \sum_{\theta_{rx}} \mathrm{APS}(\theta_{rx}, \theta_{tx}, \tau) \tag{5}$$

where $N_{\theta_{tx}} = 360$ and $N_{\theta_{rx}} = 181$ is the number of entries for θ_{tx} and θ_{rx} respectively.

IV. Scatterer mapping

In this section, a method of estimating paths from measurements and mapping their interactions to physical scatterers (walls and objects) is described. Although high resolution methods like Unitary ESPRIT [40] and SAGE [41] can provide more details, a more robust non-parametric beam scanning approach is chosen in this work in order to avoid possible problems due to model-mismatch and non-ideal measurements. The beam-scanning described above is used to estimate the path properties, then the paths are grouped across samples based on development in angles and delay. Measured delay and angle values are used as a starting point to map the interactions to the physical objects. Ray tracing is used to assist in mapping the interactions, and crucial for resolving multi bounce paths. When all paths are mapped to the objects in the environment, identifying common physical scatterers (walls/objects) among the two users is possible. The analysis and figures focuses mainly on the last bounce, the user perspective. The steps are described in the following subsections.

A. Path Estimation

A simple 3D peak search is used on the beam-scanning results of (1) to find a set of peaks within a 20 dB dynamic range. The location of those peaks determines the paths' gain, AoA, AoD and delay. An example is shown in Fig. 6 for one of six samples in a segment, where the estimated paths are shown as white circles on top of the single-sided beam-scanning spectrum seen from the Rx array. The same paths are drawn on top of the beam-scanning spectrum seen from the mobile station as depicted in Fig. 7. Paths are estimated for each of the 6 samples in each segment.

B. Path Grouping

Paths are grouped together if they have similar angle and delay across the $K = 6$ samples in a segment (Fig. 4). The grouping is based on the minimum distance in angle and delay between all paths L_k in sample k and all paths L_{k-1} in sample $k-1$. The distance matrices $D \in \mathbb{R}^{L_k \times L_{k-1}}$ are calculated as:

$$D_\tau(l_k, l_{k-1}) = |(\tau_{l_k} - \tau_{l_{k-1}})| \tag{6}$$

$$D_\theta(l_k, l_{k-1}) = |(\theta_{l_k} - \theta_{l_{k-1}})| \tag{7}$$

A threshold ϵ_τ and ϵ_θ of $4\,\mathrm{ns}$ and 4° was used for a maximum distance in angle and delay before the paths are not

This article has been accepted for publication in IEEE Transactions on Antennas and Propagation. This is the author's version which has not been fully edited and content may change prior to final publication. Citation information: DOI 10.1109/TAP.2021.3111411

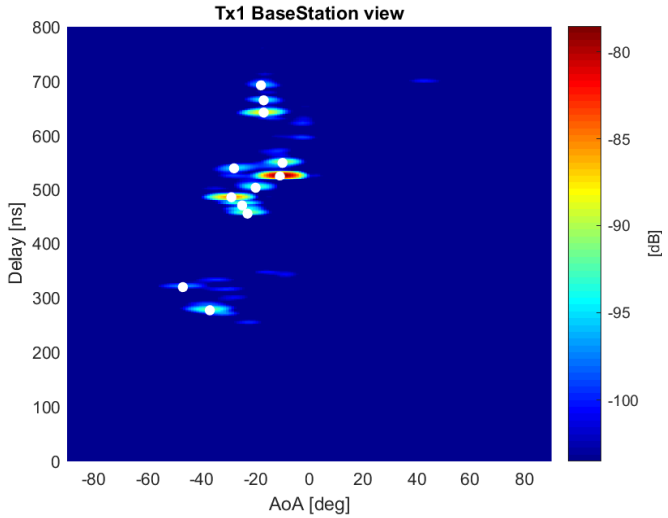

Fig. 6: Peaks of paths from angular delay profile of TX1 seen from base station. The corresponding mobile station perspective is shown in Fig. 7.

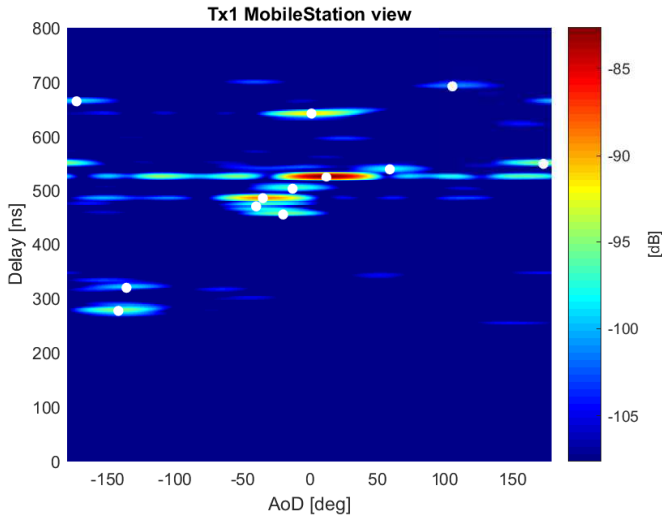

Fig. 7: Peaks of paths from angular delay profile of TX1 seen from mobile-station. The correcsponding base station perspective is shown in Fig. 6.

grouped by minimum distance. These thresholds were obtained by experiments on the data to find the most robust grouping for inspecting and correcting multibounce paths in later steps. For initialization, all L paths in the first sample are assigned a unique group id G, and then paths in sample 2 are compared to sample 1 for minimal distance. Every matching paths are assigned the same group id as its matching path l_{k-1}. Any paths that are not matched between samples k and $k-1$ means the paths have died and/or was (re)born. (Re)born paths are compared to the most recent value of dead paths for possible matching criteria and rebirth of paths. If there is no match with dead paths, it is considered born, and assigned a new unique group ID. The general procedure is described in Algorithm 1.

The grouping can greatly reduce the amount of manual inspection required for correcting multi bounce paths in Section IV-D. When the paths are grouped in this manner, each group represents a single path's development across the 6 samples. Fig. 8 illustrates the groups, in separate colors, as seen from the base station array in AoA and delay. For cluster tracking of measurements alone, i.e, when there is no need to simultaneously align with raytracing or environment mapping, more automated methods for cluster tracking and model generation [42]–[44] can be suitable for larger datasets.

Algorithm 1 Group paths across samples

Require: every $l_{k=1}$ is assigned unique G
  for $k = 2 : K$ **do**
    calculate D for L_k and L_{k-1} paths
    for $l_k = 1 : L_k$ **do**
      if $min(D(l_k, :)) < \epsilon_\tau \& \epsilon_\theta$ **then**
        assign $G_{l_k} \leftarrow G_{l_{k-1}}$
      else
        compute distances D' from l_k to dead groups
        if $min(D') < \epsilon_\tau \& \epsilon_\theta$ **then**
          assign $G_{l_k} \leftarrow G_{dead}$
        else
          assign new unique ID $G_{l_k} \leftarrow G_{unique}$
        end if
      end if
    end for
    any unmatched l_{k-1} is considered dead
  end for

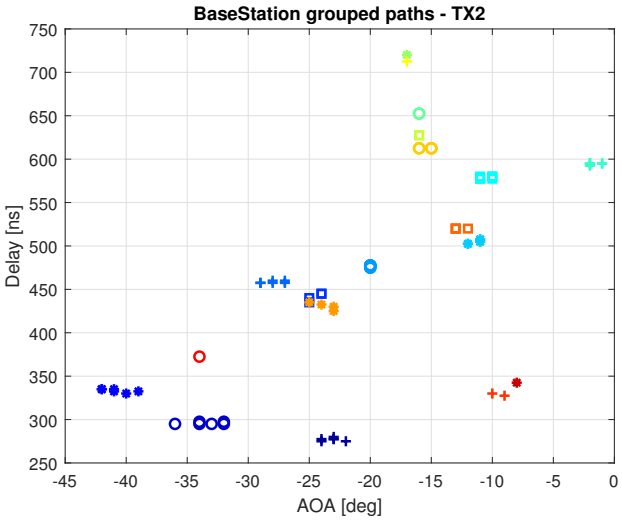

Fig. 8: Example of the evolution of path groups as seen from the base station array in AoA and delay. Colour and symbols separates the groups.

C. Ray Tracing

The tool used for ray tracing is Wireless Insite by Remcom [45]. Buildings are modeled by using data available in the public database called open street map [46], as well as manual laser height and distance measurements of buildings. Locations of Tx and Rx are given by measured distances to reference points on nearby buildings with centimetre accuracy. The

This article has been accepted for publication in IEEE Transactions on Antennas and Propagation. This is the author's version which has not been fully edited and content may change prior to final publication. Citation information: DOI 10.1109/TAP.2021.3111411

majority of measured tracks are straight lines parallel to building walls for ease of replication in RT and common coordinate systems. For simplicity in the simulations, the Tx and Rx are placed at the center of the arrays and only one element is simulated. The Tx is assigned an isotropic pattern, while the Rx is assigned a uniform pattern covering the half-sphere pointing outwards from the building. Some building details as well as trees, lamp-posts and signs etc., are left out of the simulation to limit modeling complexity. A maximum of 5 reflections and 1 diffraction is used in this simulation. The simulation results are a good match with the paths found in the measurements. The 3D model used in RT and some sample paths are depicted in Fig. 10.

D. Multi Bounce Corrections

As described above, the paths for every single sample is estimated from the wideband beam-scanning results of each of the two Tx arrays. Each path has a delay, AoA and AoD and the location of the Rx and Tx arrays are known, as well as the arrays' orientation during each measurement block.

In the initial step, each path is assumed to be single bounce paths to start estimating scatterer locations. With the known location of Tx and Rx arrays as well as the AoA and total delay, there can only be one solution for the placement of the scatterer. The AoA is used here since the Rx array is fixed during all measurements, and is less prone to directional errors as the shaking and moving of the Tx arrays (AoD). An example of the scatterers locations found using this single bounce assumption is plotted in Fig. 9 for Tx2 in position 4.

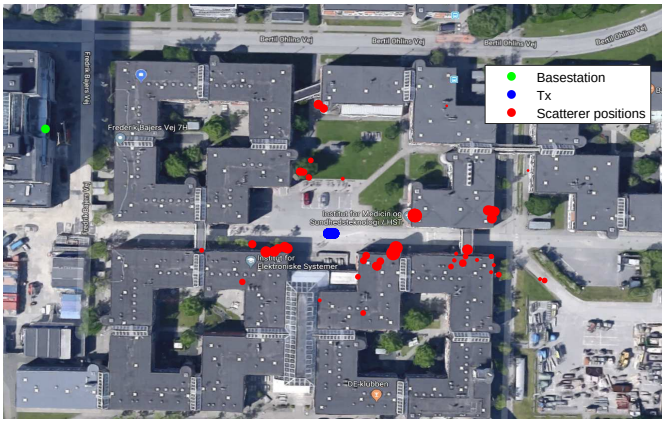

Fig. 9: Location of scatterers using only the single bounce assumption for placement. The larger size of each circle indicates higher path gain. Image by Google Maps.

The red scatter points in Fig. 9 have different size according to each path's gain. Most of the points align very well with the walls/objects that surround the Tx array. The remaining scatter points seemingly inside the buildings are paths with two or more bounces that are not correctly placed with the single bounce assumption. To confirm single bounce paths, and correct dual or higher number bounces, RT simulation is used together with the AoA, AoD and delay from the measurements, to locate the interaction points that make up the full path. An example of RT paths for Tx2 is illustrated in Fig. 10. The figure has a limited dynamic range to better illustrate the strongest paths.

Most of the multi bounce paths are easily identified from RT simulation, but exact matches between RT and measurements are very difficult, especially when the RT model is simplified. The mismatch in ray tracing and measurement means that all paths need to undergo manual inspections and ray tracing comparison. To greatly simplify and speed up both the inspection and multi bounce correction, paths are processed in groups according to Section IV-B. An example of such a correction is illustrated in Fig. 11 where multiple paths in one group are corrected by the equivalent paths from RT. After the correction, this group of dual bounce paths now matches with measured delay, AoA and AoD.

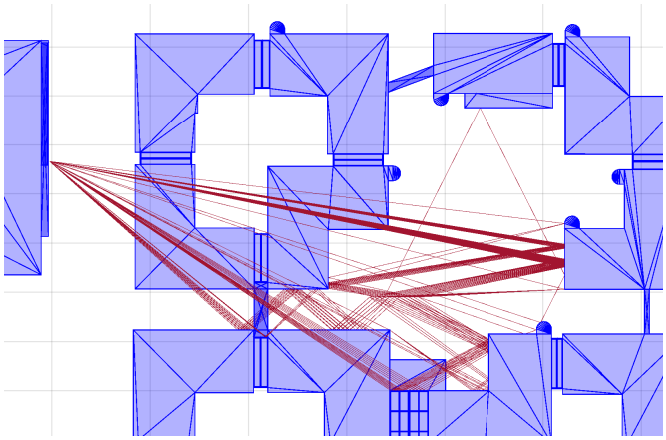

Fig. 10: An example of RT paths for a section of the Tx2 track.

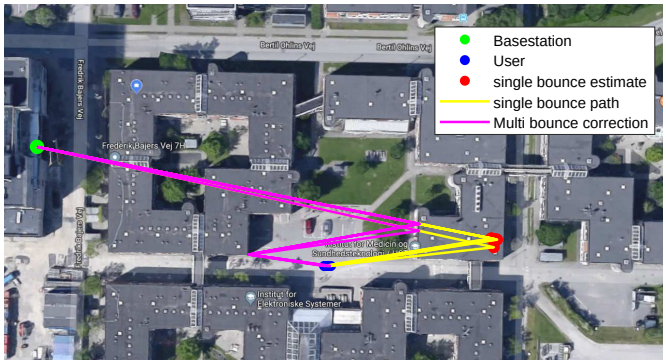

Fig. 11: Path correction for a group of paths with two bounces. Image by Google Maps.

V. Results

This section presents the results obtained from applying the procedures described above on two different pairs of measurement tracks and then compares the results to the channel correlation and distance between the users. Tx1 and Tx2 positions 1-4 are from the parallel tracks E and I from Fig.3. Positions 5-7 are from the perpendicular tracks C and D. The paths from multiple positions on two separate track

This article has been accepted for publication in IEEE Transactions on Antennas and Propagation. This is the author's version which has not been fully edited and content may change prior to final publication. Citation information: DOI 10.1109/TAP.2021.3111411

sets are obtained and multi bounces are corrected before each paths interactions are assigned to scatterers in the map. An example is shown in Fig.12, where each color represents a different wall/object association (user perspective). The walls and objects defined for interactions are displayed and numbered in Fig. 13.

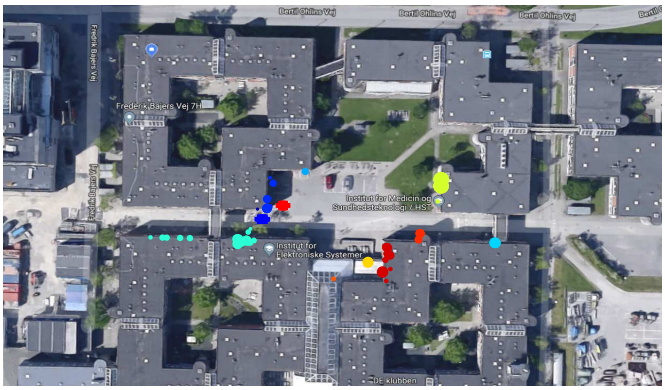

Fig. 12: Wall/object assosiation of scatterpoints. Red and blue points on the road are Tx1 and Tx2 in position 2, respectively. Image by Google Maps.

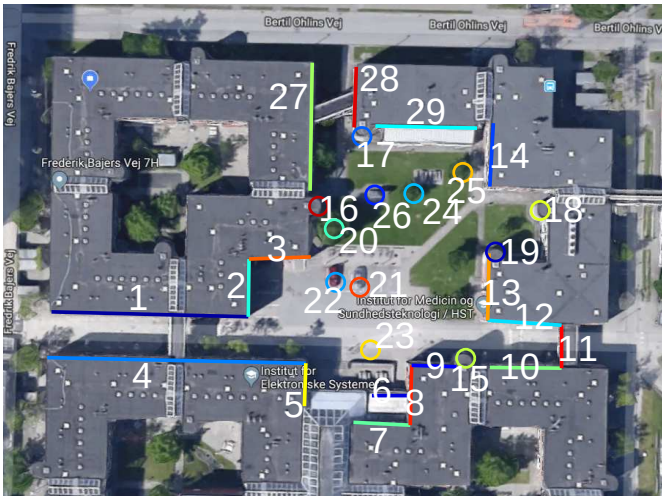

Fig. 13: Wall and object numbering. Image by Google Maps.

A. Parallel Tracks, Positions 1-4

The user arrays are moving parallel to each other in positions 1-4, Tx2 on the E-track, and Tx1 on the I-track. The power associated with each wall can be seen in Fig. 14 for each Tx. Tx1 repeats the same distance four times and the power distribution is therefore very similar across the four positions. Tx2 is analysed at four different positions along a straight track. In position 1, 28% and 67% of the power has the last bounce on walls 1 and 4 respectively, which forms a narrow street canyon. In this position the visibility of the open area is limited, and there is little contribution from other walls. Tx2 in position 2 is just entering the open area and has higher visibility of the walls inside the open space and wall 13 now accounts for a majority of Tx2's power. When Tx2 is moved further into the open area, the contribution from wall 13 is slightly reduced and other walls and objects account for larger percentages of the total power.

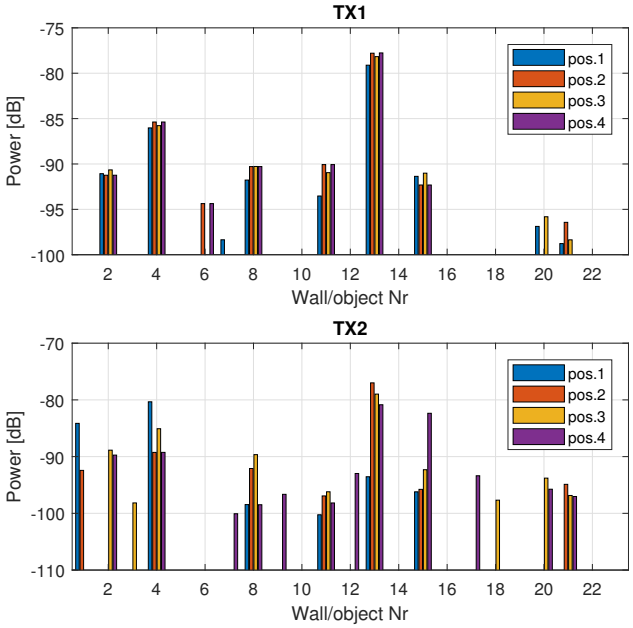

Fig. 14: Power contribution per scatterer for each of the four positions 1-4. Power is relative to transmit power.

Each path has an associated power, but also the number of bounces between Rx and Tx. The cumulative power for each Tx in all 4 positions is depicted in Fig. 15. In all but one case, more than 95% of the power is from single and dual bounce paths. In these cases, the Txs have good visibility of the open square where one or multiple single bounce paths together account for 87-95% of all paths' power. The remaining case (Tx2, pos.1) is where the Tx array is located in position 1 from Fig. 5, where the nearby building walls (no.1 and 4) enables a high number of bounces within a short extra path length inside the narrow street canyon.The remaining case (Tx2, pos.1) inside the street canyon, the nearby walls allow for additional bounces with relatively small additional path length and thus limited losses. Accounting as well for the limited visibility of the square, more significant percentages of power in paths with two and three bounces is observed.

B. Perpendicular Tracks, Positions 5-7

The two users are moving perpendicular to each other in positions 5-7, with Tx2 on C-track, and Tx1 on D-track. Positions 6 and 7 are from the same 15-second measurement block, but at two different locations. The first perpendicular position (position 5) of Tx1 and Tx2 is illustrated in Fig. 16, with their respective last bounce scatterer locations. The two users are approximately 30 m away from each other and at very different angles seen from the base station. The two users have very different sets of walls contributing as the last bounce scatterers. Similarly to the parallel tracks, the walls power contribution to each Tx in positions 5-7 are illustrated in Fig. 17. Tx1's track is now just a few meters north compared

This article has been accepted for publication in IEEE Transactions on Antennas and Propagation. This is the author's version which has not been fully edited and content may change prior to final publication. Citation information: DOI 10.1109/TAP.2021.3111411

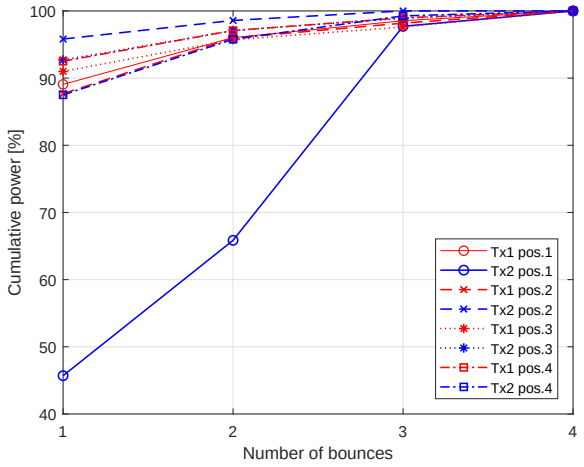

Fig. 15: Cumulative power of contributions with different number of bounces for both Tx arrays in positions 1-4

to positions 1-4, but there are large differences in which walls contribute to the user. The missing reflection from wall 13 is now blocked by a car parked close by (object 22 in Fig. 13), and wall 10 is now the dominant wall for all 3 positions.

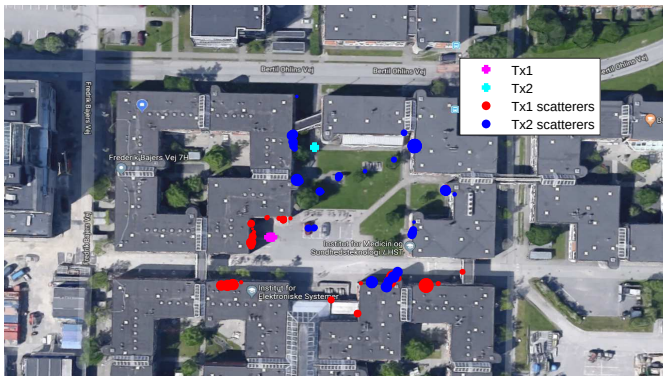

Fig. 16: Tx1 and Tx2 locations with mapped scatterers at position 5. Image by Google Maps.

Fig. 18 illustrates the cumulative power over the number of bounces for the 3 individual positions. Compared to position 1-4, Tx1 has a very low amount of power in single bounce paths, and the majority of power from dual bounce paths. The blocked reflection from wall 13 and the additional powerful dual bounce from wall 10 is contributing to the shift in the distribution for Tx1.

C. Channel Vector Orthogonality

The inner product of the vectors describing the channel from the base station to different users is crucial in MMIMO, where complete orthogonality provides optimal transmit power consumption or sum-rate channel capacity [4]. This section uses the correlation between the user channel vectors as a measure, and compares the results with the number of common scatterers observed earlier in Section V. The eight elements at the two user arrays are summed together to emulate an

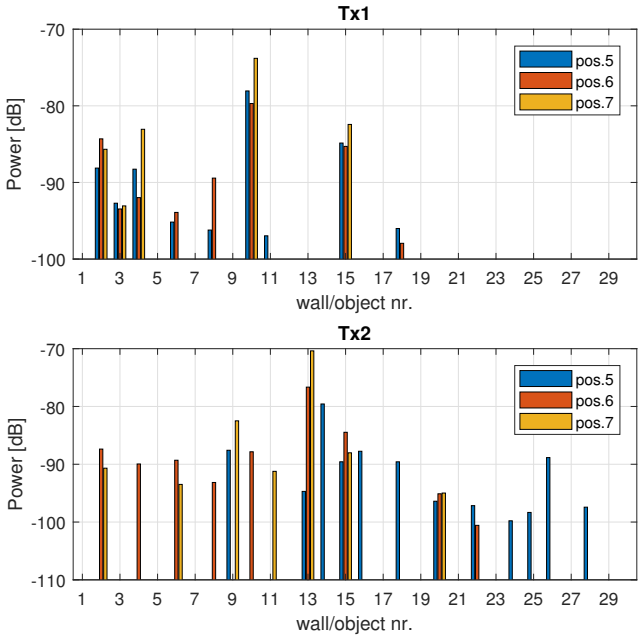

Fig. 17: Power contribution per scatterer for each of the three positions 5-7. Power is relative to transmit power.

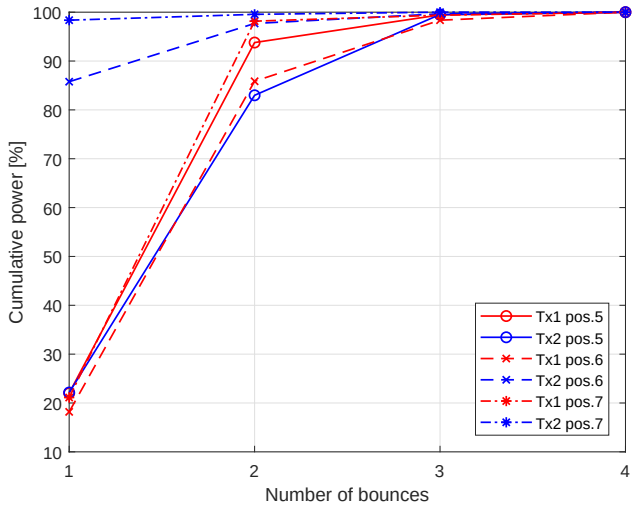

Fig. 18: Cumulative power of contributions with different number of bounces for both Tx arrays in positions 5-7

omnidirectional pattern in azimuth for each user. Considering only two users i and j, the pairwise correlation between the two channels is defined by the normalized inner product:

$$\rho_{ij} = \frac{|\mathbf{h}_i^* \mathbf{h}_j|}{\|\mathbf{h}_i\| \|\mathbf{h}_j\|} \tag{8}$$

Where $\mathbf{h}_x \in \mathbb{C}^{M \times 1}$ is the vector of M Rx antennas towards user i or j.

Fig. 19 depicts the correlation over 50 snapshots averaging sliding window for the four measurement blocks of positions 1-4. The red curve is the correlation for 16 array elements, and is the default for discussion in this section. The correlation is also displayed for 32 and 64 elements at the base station.

This article has been accepted for publication in IEEE Transactions on Antennas and Propagation. This is the author's version which has not been fully edited and content may change prior to final publication. Citation information: DOI 10.1109/TAP.2021.3111411

The numbered blue bars indicate the segments that have been analysed for common scatterers according to previous sections.

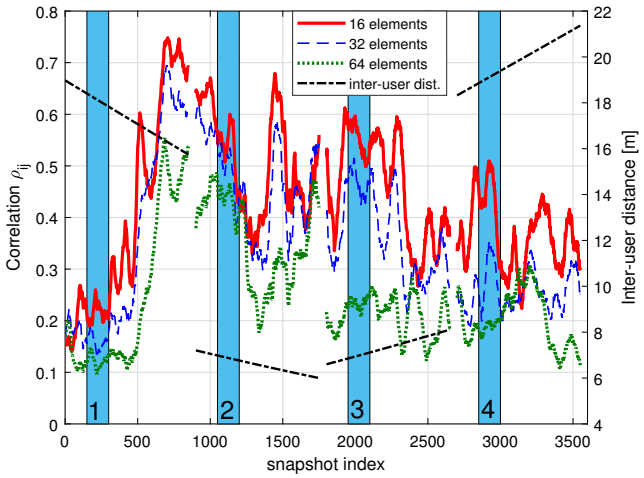

Fig. 19: Correlation of user vectors with a 50 snapshot sliding window for 16, 32 and 64 elements at the base station. Black dotted lines are inter-user distance on right Y-axis. Numbered blue bars indicate Tx positions 1-4 from E/I track, analysed for common scatterers.

The user correlation will be compared against the inter-user distances which are displayed by the black lines in Fig. 19 and 20. The inter-user distances are estimated by assuming constant walking speed and using the Tx's start and stop coordinates of each measurement block. As illustrated in Fig. 19 and 20, the location of the analysed segments in positions 1-6 are close to the start of each measurement block, and position 7 is just past the middle of a measurement block.

The first position in Fig. 19 shows a very low correlation of about 0.2, where the users are in NLOS to each other. In positions 2-4, Tx 2 moved into the open square and there is LOS between the users, and the correlation is higher ranging from 0.6 to 0.4. This is a good match with observations in Fig. 14, where both users share the majority of received power from wall 13, especially in positions 2 and 3. In position 2, the two users are almost perfectly aligned in the direction of the dominant wall 13, which means there is a very small angular separation, seen from the base station, through the dominant scatterer. Moving to position 3 and 4, the angular separation of the two users increases with respect to wall 13. The general trend is a decrease in correlation from position 2 through 4, this is consistent with the angular separation to wall 13 as well as the power shared by wall 13. The inter-user distances for the four measurement blocks in Fig. 19 are "symmetrical", with the smallest distance at the end of the second measurement block. The larger angular resolution provided by utilizing 32 and 64 antennas does not significantly decrease the correlation in position 2. The correlation is decreased with 64 antennas in position 3, and with 32 antennas in position 4 where the angular separation is larger. Larger variation in the correlation from snapshot 1000 until the end of Fig. 19, is likely in part due to shadowing of strong reflections, as trees cover part of some walls, including wall 13.

Fig. 20 illustrates the correlation for the two measurement blocks of positions 5-7. The same match between correlation and overlap in wall contribution is not as straight forward. Position 5 has a very low correlation due to the large distance and NLOS between users, and very different scatterers contribute to each user as illustrated in Fig. 16 & 17. Position 6, and especially 7 on the other hand, displays a higher correlation but no major overlap in power from common walls. The inter-user distances for both positions are between 13 and 14 meters. Tx1 receives the majority of its power from wall 10, which is reflected from wall 11. Tx2 receives the majority from wall 13 as a single bounce. Seen from the base station, these two first bounce walls are very close in angle, especially around position 7 where the correlation increased rapidly. This scenario is illustrated by the strongest path (RT) for each user in Fig. 21. The 16 elements at the base station are not fully able to separate the users, but utilizing 32 or 64 elements at the base station greatly decreases the correlation for positions 6 and 7. The 4 modules individually see the same large clusters for this position, so the reduced correlation is achieved mainly by increased angular resolution. Across all measurements in Fig. 19 and 20, increasing the amount of elements at the base station typically decreases the correlation.

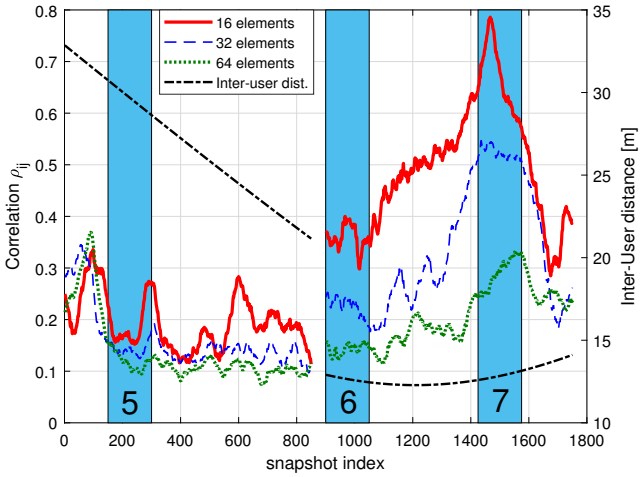

Fig. 20: Correlation of user vectors with a 50 snapshot sliding window for 16, 32 and 64 elements at the base station. Black dotted lines are inter-user distance on right Y-axis. Numbered blue bars indicate Tx positions 5-7 from C/D track, analysed for common scatterers.

VI. Discussion

The positions analysed in this paper provide different distances between users, as well as different angles with respect to scattering objects. In 2 out of 7 positions (1 and 5) the users do not have a line of sight to each other. For these positions we observe very low user correlation. In the remaining positions with LOS between the users, varying levels of angular separation and inter-user distance impacts user correlation.

For the NLOS scenarios investigated in this paper, the criteria for cluster sharing or channel correlation can be shown to be dependent on more than simply the unidirectional

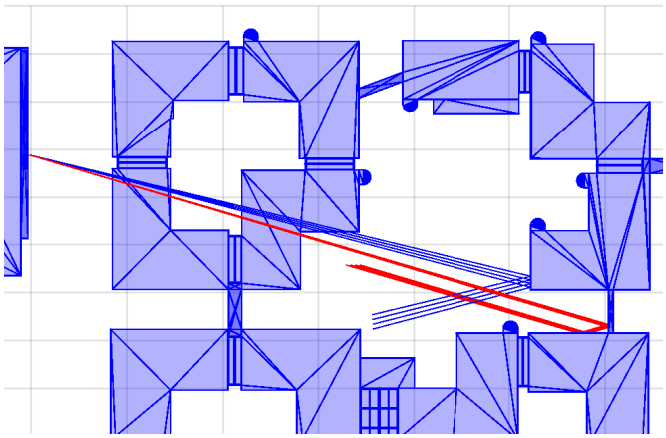

Fig. 21: Simulated strongest paths for Tx1 (red) and Tx2 (blue) along 4 samples of measurement block for position 6 & 7.

separation of the users. As seen in Fig. 12 and 17, the users typically see one dominant and one to two less dominant walls or clusters, which is not a very rich scattering environment. If the users line up to have very similar AoA and AoD through the dominant cluster, the channels will be more correlated. The observations indicate that the angle separation, as seen from the base station, of dominant clusters towards the users are highly important for the user correlation.

The visibility regions and distance criteria in Cost2100 and Quadriga extensions enable correlation of clusters and multi path components in multi-user scenarios based on inter-user distance. But for improved multi-user accuracy without resorting to fully deterministic models, the clusters would ideally have physical locations. This would enable simplified RT to determine the size, shape and location of more realistic VRs in the simulation area. The VRs and location of their clusters need to consider the higher correlation when any users line up in the direction of a cluster. If the simple RT simulations of VRs are not viable computationally or complexity wise, the typically circular shapes of VR could be designed for higher correlation when any two users align in direction of the cluster location. In Winner and Quadriga type models, the clusters do not have physical locations, but are defined by the AoA's and AoD's. The distance criteria proposed for Quadriga in [33] could be extended to increase the cluster sharing when the users align to the AoA of a cluster. In this way the angular separation is weighted in addition to the distance. Note that the results are based on measurements for a vertically-polarized setup and would need to be confirmed for other types of arrays, e.g., dual-polarized arrays.

VII. Conclusions

This paper presented a large outdoor MMIMO measurement campaign with dual-directional angular discrimination and two simultaneously moving user arrays. Paths were estimated from wideband dual directional beam-scanning, and with ray tracing assistance, a method of mapping single and multi bounce paths to the surrounding environment were presented. The amount of shared power per wall between the users was compared with correlation levels and inter-user distances. A good agreement between the correlation and the power of shared scatterers, either in the first or last bounce, was found. With few dominant paths for each user, the angular separation of users with respect to clusters and angular separation of clusters with respect to the base station is found to impact correlation levels. The inter-user distances are still relevant, but not observed to be a dominating factor for the investigated scenarios. The amount of power from shared walls and objects are the dominant factors, and is linked to whether the users align in the direction of the dominant scatterers, or if separate dominant scatterers are close in angle as seen from the base station. In order to introduce this important aspect into cluster based models, users lining up in the direction of a cluster should have stronger correlation of multi path components from said cluster.

Acknowledgment

The authors would like to thank Huawei Sweden AB for their financial support.

References

[1] F. Boccardi, R. W. Heath, A. Lozano, T. L. Marzetta, and P. Popovski, "Five disruptive technology directions for 5g," *IEEE Communications Magazine*, vol. 52, no. 2, pp. 74–80, February 2014.

[2] F. Rusek, D. Persson, B. K. Lau, E. G. Larsson, T. L. Marzetta, O. Edfors, and F. Tufvesson, "Scaling up mimo: Opportunities and challenges with very large arrays," *IEEE Signal Processing Magazine*, vol. 30, no. 1, pp. 40–60, Jan 2013.

[3] E. G. Larsson, O. Edfors, F. Tufvesson, and T. L. Marzetta, "Massive MIMO for next generation wireless systems," *IEEE Communications Magazine*, vol. 52, no. 2, pp. 186–195, February 2014.

[4] T. L. Marzetta, "Noncooperative cellular wireless with unlimited numbers of base station antennas," *IEEE Transactions on Wireless Communications*, vol. 9, no. 11, pp. 3590–3600, November 2010.

[5] V. Kristem, S. Sangodoyin, C. U. Bas, M. Käske, J. Lee, C. Schneider, G. Sommerkorn, C. J. Zhang, R. S. Thomä, and A. F. Molisch, "3d mimo outdoor-to-indoor propagation channel measurement," *IEEE Transactions on Wireless Communications*, vol. 16, no. 7, pp. 4600–4613, 2017.

[6] J. Zhang, Z. Zheng, Y. Zhang, J. Xi, X. Zhao, and G. Gui, "3d mimo for 5g nr: Several observations from 32 to massive 256 antennas based on channel measurement," *IEEE Communications Magazine*, vol. 56, no. 3, pp. 62–70, March 2018.

[7] X. Gao, O. Edfors, F. Tufvesson, and E. G. Larsson, "Massive mimo in real propagation environments: Do all antennas contribute equally?" *IEEE Transactions on Communications*, vol. 63, no. 11, pp. 3917–3928, 2015.

[8] J. Huang, C. Wang, R. Feng, J. Sun, W. Zhang, and Y. Yang, "Multi-frequency mmwave massive mimo channel measurements and characterization for 5g wireless communication systems," *IEEE Journal on Selected Areas in Communications*, vol. 35, no. 7, pp. 1591–1605, 2017.

[9] J. Flordelis, F. Rusek, X. Gao, G. Dahman, O. Edfors, and F. Tufvesson, "Spatial separation of closely-located users in measured massive mimo channels," *IEEE Access*, vol. 6, pp. 40 253–40 266, 2018.

[10] J. Flordelis, X. Gao, G. Dahman, F. Rusek, O. Edfors, and F. Tufvesson, "Spatial separation of closely-spaced users in measured massive multi-user mimo channels," in *2015 IEEE International Conference on Communications (ICC)*, 2015, pp. 1441–1446.

[11] À. O. Martínez, E. D. Carvalho, and J. Ø. Nielsen, "Towards very large aperture massive MIMO: A measurement based study," in *2014 IEEE Globecom Workshops (GC Wkshps)*, Dec 2014, pp. 281–286.

[12] J. Laurila, K. Kalliola, M. Toeltsch, K. Hugl, P. Vainikainen, and E. Bonek, "Wideband 3d characterization of mobile radio channels in urban environment," *IEEE Transactions on Antennas and Propagation*, vol. 50, no. 2, pp. 233–243, 2002.

[13] M. Toeltsch, J. Laurila, K. Kalliola, A. F. Molisch, P. Vainikainen, and E. Bonek, "Statistical characterization of urban spatial radio channels," *IEEE Journal on Selected Areas in Communications*, vol. 20, no. 3, pp. 539–549, 2002.

[14] K. Kalliola, H. Laitinen, P. Vainikainen, M. Toeltsch, J. Laurila, and E. Bonek, "3-d double-directional radio channel characterization for urban macrocellular applications," *IEEE Transactions on Antennas and Propagation*, vol. 51, no. 11, pp. 3122–3133, 2003.

[15] J.-M. Conrat and P. Pajusco, "Directional propagation channel estimation and analysis in urban environment with panoramic photography," *International Journal of Microwave and Wireless Technologies*, pp. 3 – 13, Feb. 2012. [Online]. Available: https://hal.archives-ouvertes.fr/hal-00704166

[16] J. Chen, X. Yin, X. Cai, and S. Wang, "Measurement-based massive mimo channel modeling for outdoor los and nlos environments," *IEEE Access*, vol. 5, pp. 2126–2140, 2017.

[17] X. Gao, F. Tufvesson, O. Edfors, and F. Rusek, "Measured propagation characteristics for very-large mimo at 2.6 ghz," in *2012 Conference Record of the Forty Sixth Asilomar Conference on Signals, Systems and Computers (ASILOMAR)*, Nov 2012, pp. 295–299.

[18] S. Payami and F. Tufvesson, "Channel measurements and analysis for very large array systems at 2.6 ghz," in *2012 6th European Conference on Antennas and Propagation (EUCAP)*, March 2012, pp. 433–437.

[19] H. Q. Ngo and E. G. Larsson, "Blind estimation of effective downlink channel gains in massive mimo," in *2015 IEEE International Conference on Acoustics, Speech and Signal Processing (ICASSP)*, April 2015, pp. 2919–2923.

[20] Da-Shan Shiu, G. J. Foschini, M. J. Gans, and J. M. Kahn, "Fading correlation and its effect on the capacity of multielement antenna systems," *IEEE Transactions on Communications*, vol. 48, no. 3, pp. 502–513, March 2000.

[21] Chen-Nee Chuah, D. N. C. Tse, J. M. Kahn, and R. A. Valenzuela, "Capacity scaling in mimo wireless systems under correlated fading," *IEEE Transactions on Information Theory*, vol. 48, no. 3, pp. 637–650, March 2002.

[22] X. Gao, O. Edfors, F. Rusek, and F. Tufvesson, "Massive mimo performance evaluation based on measured propagation data," *IEEE Transactions on Wireless Communications*, vol. 14, no. 7, pp. 3899–3911, July 2015.

[23] Chia-Chin Chong, Chor-Min Tan, D. I. Laurenson, S. McLaughlin, M. A. Beach, and A. R. Nix, "A new statistical wideband spatio-temporal channel model for 5-ghz band wlan systems," *IEEE Journal on Selected Areas in Communications*, vol. 21, no. 2, pp. 139–150, Feb 2003.

[24] Q. H. Spencer, B. D. Jeffs, M. A. Jensen, and A. L. Swindlehurst, "Modeling the statistical time and angle of arrival characteristics of an indoor multipath channel," *IEEE Journal on Selected Areas in Communications*, vol. 18, no. 3, pp. 347–360, March 2000.

[25] L. Raschkowski, P. Kyösti, K. Kusume, T. Jämsä, V. Nurmela, A. Karttunen, A. Roivainen, T. Imai, J. Järveläinen, J. Medbo, J. Vihriälä, J. Meinilä, K. Haneda, V. Hovinen, J. Ylitalo, N. Omaki, A. Hekkala, R. Weiler, and M. Peter, "Metis channel models, deliverable 1.4," Tech. Rep. ICT-317669, 2015. [Online]. Available: https://metis2020.com/

[26] P. Kyösti, J. Meinilä, L. Hentila, X. Zhao, T. Jämsä, C. Schneider, M. Narandzic, M. Milojević, A. Hong, J. Ylitalo, V.-M. Holappa, M. Alatossava, R. Bultitude, Y. Jong, and T. Rautiainen, "Winner ii channel models," *IST-4-027756 WINNER II D1.1.2 V1.2*, 02 2008.

[27] P. Heino, J. Meinilä, P. Kyösti, L. Hentila, T. Jämsä, E. Suikkanen, E. Kunnari, and M. Narandzic, "Cp5-026 winner+ d5.3 v1.0 winner+ final channel models," 01 2010.

[28] 3GPP TR 38.901, "Study on channel model for frequencies from 0.5 to 100 GHz ," Tech. Rep., January 2018.

[29] L. Liu, C. Oestges, J. Poutanen, K. Haneda, P. Vainikainen, F. Quitin, F. Tufvesson, and P. D. Doncker, "The cost 2100 mimo channel model," *IEEE Wireless Communications*, vol. 19, no. 6, pp. 92–99, December 2012.

[30] S. Jaeckel, L. Raschkowski, K. Börner, and L. Thiele, "Quadriga: A 3-d multi-cell channel model with time evolution for enabling virtual field trials," *IEEE Transactions on Antennas and Propagation*, vol. 62, no. 6, pp. 3242–3256, June 2014.

[31] X. Gao, J. Flordelis, G. Dahman, F. Tufvesson, and O. Edfors, "Massive mimo channel modeling - extension of the cost 2100 model," 2015, joint NEWCOM/COST Workshop on Wireless Communications (JNCW) ; Conference date: 14-10-2015 Through 15-10-2015.

[32] J. Flordelis, X. Li, O. Edfors, and F. Tufvesson, "Massive mimo extensions to the cost 2100 channel model: Modeling and validation," *IEEE Transactions on Wireless Communications*, vol. 19, no. 1, pp. 380–394, 2020.

[33] À. O. Martínez, P. Eggers, and E. D. Carvalho, "Geometry-based stochastic channel models for 5G: Extending key features for massive MIMO," in *2016 IEEE 27th Annual International Symposium on Personal, Indoor, and Mobile Radio Communications (PIMRC)*, Sept 2016, pp. 1–6.

[34] A. Karstensen, J. Ø. Nielsen, P. C. F. Eggers, E. De Carvalho, G. F. Pedersen, M. Alm, and G. Steinböck, "Multiuser correlation and sum-rate in outdoor measured massive mimo channels," *IEEE Antennas and Wireless Propagation Letters*, vol. 19, no. 3, pp. 433–437, 2020.

[35] M. Steinbauer, A. Molisch, and E. Bonek, "The double-directional radio channel," *IEEE Antennas and Propagation Magazine*, vol. 43, no. 4, pp. 51–63, 2001.

[36] S. Zhang, T. L. Jensen, O. Franek, P. C. F. Eggers, C. Byskov, and G. F. Pedersen, "Investigation of a UWB wind turbine blade deflection sensing system with a tip antenna inside a blade," *IEEE Sensors Journal*, no. 22, pp. 7892–7902, Nov 2016.

[37] J. Ø. Nielsen, W. Fan, P. C. F. Eggers, and G. F. Pedersen, "A channel sounder for massive mimo and mmwave channels," *IEEE Communications Magazine*, vol. 56, no. 12, pp. 67–73, December 2018.

[38] N. Czink, X. Yin, H. OZcelik, M. Herdin, E. Bonek, and B. H. Fleury, "Cluster characteristics in a mimo indoor propagation environment," *IEEE Transactions on Wireless Communications*, vol. 6, no. 4, pp. 1465–1475, April 2007.

[39] MVG. Multi-probe systems - sg 24. Accessed on: 9. April 2020. [Online]. Available: https://www.mvg-world.com/en/products/antenna-measurement/multi-probe-systems/sg-24

[40] M. D. Zoltowski, M. Haardt, and C. P. Mathews, "Closed-form 2-d angle estimation with rectangular arrays in element space or beamspace via unitary esprit," *IEEE Transactions on Signal Processing*, vol. 44, no. 2, pp. 316–328, 1996.

[41] B. H. Fleury, M. Tschudin, R. Heddergott, D. Dahlhaus, and K. Ingeman Pedersen, "Channel parameter estimation in mobile radio environments using the sage algorithm," *IEEE Journal on Selected Areas in Communications*, vol. 17, no. 3, pp. 434–450, 1999.

[42] N. Czink, R. Tian, S. Wyne, F. Tufvesson, J. Nuutinen, J. Ylitalo, E. Bonek, and A. F. Molisch, "Tracking time-variant cluster parameters in mimo channel measurements," in *2007 Second International Conference on Communications and Networking in China*, 2007, pp. 1147–1151.

[43] N. Czink, T. Zemen, J.-P. Nuutinen, J. Ylitalo, and E. Bonek, "A time-variant mimo channel model directly parametrised from measurements," *EURASIP Journal on Wireless Communications and Networking*, vol. 2009, no. 1, 2009.

[44] N. Czink, E. Bonek, L. Hentila, J. Nuutinen, and J. Ylitalo, "A measurement-based random-cluster mimo channel model," in *2007 IEEE Antennas and Propagation Society International Symposium*, 2007, pp. 5363–5366.

[45] Remcom. Wireless insite. Accesed on: june 2019. [Online]. Available: https://www.remcom.com/

[46] OpenStreetMap contributors. (2017) Planet dump retrieved from https://planet.osm.org . Accessed on: june 2019. [Online]. Available: https://www.openstreetmap.org

Anders Karstensen received his bachelor in electronic engineering from University of Agder, Norway, in 2013. He received his M.Sc. and Ph.D degrees from Aalborg University, Denmark, in 2015 and 2020 respectively. He is currently with the department of Electronic systems, Aalborg university, Denmark. His main research interests are in Massive MIMO channel measurements and modelling, millimeter wave channels, and ray-tracing simulations.

This article has been accepted for publication in IEEE Transactions on Antennas and Propagation. This is the author's version which has not been fully edited and content may change prior to final publication. Citation information: DOI 10.1109/TAP.2021.3111411

Jesper Ø. Nielsen received the master's degree in electronics engineering and the Ph.D. degree from Aalborg University, Denmark, in 1994 and 1997, respectively. He is currently with the Department of Electronic Systems, Aalborg University, Denmark, in the antennas, propagation, and millimeter-wave systems section. His main areas of interest include experimental investigation of the mobile radio channel and the influence mobile device users have on the channel. Among other things, he has been involved in massive MIMO and mm-wave channel sounding and modeling, as well as measurements using live LTE networks. In addition, he has been working with radio performance evaluation, including over the air testing of active wireless devices.

Patrick C. F. Eggers was born in Stockholm, Sweden, in 1957. He received the M.Sc.E.E. and Ph.D. degrees from Aalborg University, Aalborg, Denmark, in 1984 and 2003, respectively. Since 1984, he has been a full-time Researcher with Aalborg University, mainly within wireless radio communications, where he is currently an Associate Professor with the Antennas, Propagation and Millimetre-Wave Systems Section. From 1988 to 1989, he was with Telecom New Zealand, Wellington, New Zealand, where he was involved in multidiffraction path-loss modeling. He has been responsible for the planning and analysis of propagation work in domestic and EU projects like TSUNAMI and CELLO. He was an active participant in a sequence of wireless communications related COST actions, starting from COST207. He is the initiator of the established English-taught international M.Sc.E.E. course at Aalborg University, specializing in wireless communication. His current research interests include propagation and wireless communications, angular propagation characteristics related to multiantenna system operation (massive multi-in multi-out) and statistical channel modeling, for example, for ultrareliable communications, and channel characterization in harsh environments relevant for the TETRA system or sensor-based systems with nearfield disturbances.

Elisabeth De Carvalho received the Ph.D. degree in Electrical Engineering from Telecom ParisTech, France. After her Ph.D. degree, she was a Post-Doctoral Fellow at Stanford University, Stanford, CA, USA, and then worked in industry in the field of DSL and wireless LAN. Since 2005, she has been with Aalborg University, where she is a Professor and has led several research projects in wireless communications. She has co-authored the book "A Practical Guide to MIMO Radio Channel". Her main expertise is in the field of signal processing with emphasis on MIMO communications. She is a member of IEEE Signal Processing Society, technical committee "Signal Processing for Communications and Networking" (SPCOM) and vice chair of the IEEE COMSOC Emerging Technology Initiative on Machine Learning for Communications. She is an associate editor of IEEE Transactions of Wireless Communications. She is the coordinator of the European Union H2020 Innovative Training Network WindMill focusing on machine learning for wireless communications.

Gert F. Pedersen Gert Frølund Pedersen (Senior Member, IEEE) was born in 1965. He received the B.Sc. and E.E. (Hons.) degrees in electrical engineering from the College of Technology in Dublin, Dublin Institute of Technology, Dublin, Ireland, in 1991, and the M.Sc.E.E. and Ph.D. degrees from Aalborg University, Aalborg, Denmark, in 1993 and 2003, respectively. Since 1993, he has been with Aalborg University, where he is currently a Full Professor heading the Antennas, Propagation, and Millimeter-wave Systems LAB with 25 researchers. He is also the Head of the Doctoral School on wireless communication with some 40 Ph.D. students enrolled. He has published more than 500 peer-reviewed articles, six books, 12 book chapters, and holds over 50 patents. He has also worked as a Consultant for developments of more than 100 antennas for mobile terminals including the first internal antenna for mobile phones in 1994 with lowest SAR, first internal triple-band antenna in 1998 with low SAR and high TRP and TIS, and lately various multiantenna systems rated as the most efficient on the market. He has worked most of the time with joint university and industry projects and have received more than 21 M in direct research funding. He is also the Project Leader of the RANGE project with a total budget of over 8 M investigating high performance centimeter/millimeter-wave antennas for 5G mobile phones. He has been one of the pioneers in establishing over-the-air measurement systems. The measurement technique is now well established for mobile terminals with single antennas. He was chairing the various COST groups with liaison to 3GPP and CTIA for over-the-air test of MIMO terminals. He is also involved in MIMO OTA measurement. His research interests include radio communication for mobile terminals especially small antennas, diversity systems, propagation, and biological effects.

Martin Alm received his M.Sc. in Electrical Engineering from Chalmers University of Technology, Sweden in 1995. Since then he has worked at Ericsson and Huawei with antennas, propagation and signal processing in radar and wireless communication contexts. Currently his main research interest is Massive MIMO system design.

Gerhard Steinböck received the DI (FH) degree in telecommunications from Technikum Wien, Austria in 1999. From 2000 to 2006, he worked as a R&D engineer at the Austrian Institute of Technology (AIT), Vienna, Austria, contributing among other things in the hard- and software development of a real-time radio channel emulator. Gerhard Steinböck received the M.Sc.E. *(cum laude)* and the Ph.D. degree in wireless communications from Aalborg University, Denmark, in 2008 and 2013, respectively. After continuing as a postdoctoral researcher at Aalborg University, Gerhard Steinböck joined Huawei Technologies Sweden AB in 2016. His research interests lie in the area of wireless communications, systems simulation, radio channel modeling, radio channel estimation and sounding, and radio geolocation techniques.